Design guideline of capacitive power transfer system to achieve targeted output power

Supapong Nutwong, Ekkachai Mujjalinvimut, Anawach Sangswang, Nattapong Hatchavanich, Mongkol Konghirun
Department of Electrical Engineering, King Mongkut's University of Technology Thonburi, Bangkok, Thailand

Article Info	ABSTRACT
	Power transfer capability of the capacitive power transfer (CPT) system is dependent on the dimensions of capacitive coupler, which should be correctly designed to meet the required amount of output power. This paper presents a guideline to design the conductive plates used in CPT system to achieve a targeted output power. For a given operating frequency, resonant inductance, DC input voltage, load resistance, and the air gap between plates, the required cross-sectional area of conductive plates is obtained using this guideline. It has been guided through the design procedure which is explained in detail. A step-by-step guide to design a 5-watts CPT system is demonstrated as a design example. The proposed design guideline is verified by the experiment which shows the closeness between measured and targeted output power. Design error is obtained as low as 3.6 percent.

Corresponding Author:

Ekkachai Mujjalinvimut
Department of Electrical Engineering, King Mongkut's University of Technology Thonburi
126 Pracha Uthit Rd., Bang Mod, Thung Khru, Bangkok, 10140, Thailand
Email: ekkachai.muj@kmutt.ac.th

1. INTRODUCTION

Wireless power transfer (WPT) is a technique to transmit electric power without any electrical wiring between source and load, which was first presented by Nikola Tesla in the 1907. After that, it has been extensively studied by many researchers. Its inherent galvanic isolation drives this technique to become popular nowadays. It is widely used in different wireless charging applications [1]–[7]. Recent development in this technology is the ability to transfer power and data simultaneously [8]–[10].

The WPT technique can be categorized by its working principle as inductive power transfer (IPT) and capacitive power transfer (CPT). In IPT, the electric power is wirelessly transferred through the magnetic field, while the electric field is used as the transfer medium in CPT. The power losses, weight, and electromagnetic interference (EMI) of the CPT system are lower compared to the IPT system. Therefore, it has gained much attention in recent years [11]–[13]. The CPT technique has been found in various applications, especially in biomedical implants [14]–[19]. Its further applications are electric vehicles [20]–[22], unmanned aerial vehicles (UAVs) [23]–[25], autonomous underwater vehicles (AUVs) [26], portable devices [27], and rotary applications [28].

To enhance the performance of CPT system, the analysis and design of this system has been presented in previous research. For example, the optimum design algorithm to achieve desired power transfer efficiency (PTE) of CPT system for biomedical implants is proposed in [29]. The analysis and design of CPT system with multiple-input multiple-output (MIMO) capacitive couplers is introduced in [30] to increase the power transfer capability of single-input single-output (SISO) couplers. Design and analysis of a flexible capacitive coupler using thin copper foil is proposed to serve the applications with flexible

requirement in [31]. The analysis and design of multiple-output CPT system for low-power portable devices is presented in [32] where the independence of power transfer to different receivers with reduced plate voltage is achieved. The double-side LCLC-compensated CPT converter is designed in [33] to meet the predesigned voltage stress across the coupler plates. Design of the CPT system with multiple receivers is presented [34] to obtain a constant voltage output against load variation and pickups removal. The resonant inverter used in CPT system is designed in [35] to maintain efficiency during the misalignment between coupler plates. For underwater applications, the four-plate CPT system is analyzed and designed in [36] to obtain a stable output voltage and power.

However, the aforementioned research uses the already provided capacitive coupler where the detail of capacitive plate design is absent. Moreover, the design of plate area has never been reported in the literature. Therefore, this paper presents the design guideline of capacitive couplers used in CPT system. The cross-sectional area of conductive plates required to achieve a targeted output power is designed according to a given operating frequency, resonant inductance, DC input voltage, load resistance, and the air gap between plates. The design procedure is presented and explained in detail. An example of designing a 5 W CPT system is also introduced, which is verified by the experiment.

2. SYSTEM ANALYSIS

2.1. System description

The capacitive power transfer system under studied is shown in Figure 1, which consists of DC voltage source (V_{dc}), inverter circuit, capacitive coupler, LC resonant tank, and a resistive load (R_L). Four MOSFET switches (S_1–S_4) form a full-bridge inverter, which is used to convert a smooth DC voltage into a high frequency square wave voltage (V_{in}). Four conductive plates (P_1, P_2, P_3, and P_4) are adopted to construct a capacitive coupler. Plate P_1 and P_2 are located on the primary-side (transmitter-side) whereas P_3 and P_4 are located on secondary-side (receiver-side). The air gap between P_1-P_3 and P_2-P_4 creates two parallel-plate capacitors, which are the main coupling capacitor of this system. Note that, in this studied system, the position of all conductive plates is fixed throughout the operation where plate P_1 is perfectly aligned with P_3 and plate P_2 is perfectly aligned with P_4. Resonant inductors (L_{R1} and L_{R2}) and resonant capacitors (C_{R1} and C_{R2}) are introduced in both primary and secondary circuits to construct a double-side LC compensation topology. These LC resonant tanks are used to compensate for the reactive power required by the capacitive coupler and to enable the resonant operation.
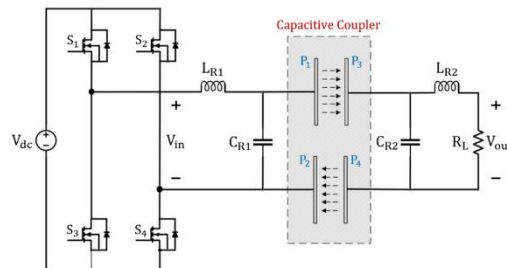

Figure 1. Capacitive power transfer system under studied

2.2. Capacitive coupler

Construction of the capacitive coupler used in this studied system is based on the parallel-plate capacitor as illustrated in Figure 2. Its capacitance is dependent on the cross-sectional area of the plate (A), distance between the plate (d), and the relative permittivity (ε_r) of material used for a dielectric which can be expressed as (1),

$$C = \frac{\varepsilon_o \varepsilon_r A}{d} \tag{1}$$

where $\varepsilon_o = 8.854 \times 10^{-12}$ (F/m) is the permittivity of free space. From (1), the area of conductive plate can be derived as:

$$A = \frac{Cd}{\varepsilon_o \varepsilon_r} \tag{2}$$

The capacitance obtained from (1) is defined as ideal capacitance due to the edge-effect not being taken into account. However, as discussed in [37], real (practical) capacitance will be comparable to ideal capacitance if the plate length (l) is much larger than the distance between plates (d). Therefore, the parallel-plate capacitor with narrow air gap is considered in the studied system. For a square metal plate, the plate length is equal to square root of plate area ($l = \sqrt{A}$).
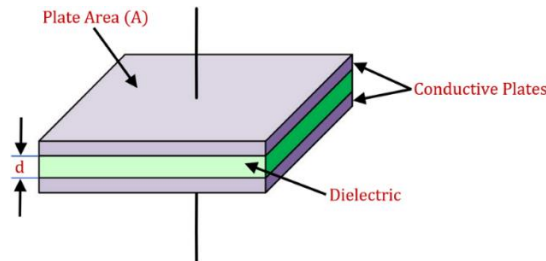

Figure 2. Construction of the parallel-plate capacitor

In this work, four square conducting plates with the arrangement as shown in Figure 1 are adopted as the capacitive coupler. It creates six capacitors in the practical operation as shown in Figure 3 where C_{13} and C_{24} are main coupling capacitors, C_{14} and C_{23} are cross-coupling capacitors, C_{12} and C_{34} are leakage capacitors. The value of these capacitors can be obtained by experimental measurement. It is noted that the main coupling capacitance can also be calculated using (1). Since the cross-sectional area (A) of all conductive plates are identical and the air gap (d) between P_1-P_3 and P_2-P_4 are the same, the main coupling capacitance of the four-plates capacitive coupler are ideally equal ($C_{13}=C_{24}$). From the experimental results of some previous researches as presented in [38]–[40], the cross-coupling capacitance and leakage capacitance are much lower than the main coupling capacitance. Therefore, these capacitances can be neglected which simplifies the analysis and design of CPT system consisting with four-plates capacitive coupler.
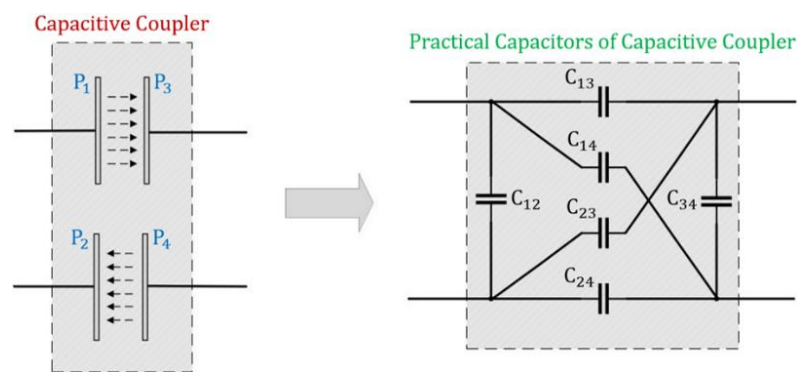

Figure 3. Practical capacitors existed in the four-plates capacitive coupler

2.3. Circuit analysis

The simplified equivalent circuit of capacitive power transfer system under studied is shown in Figure 4, based on the mutual capacitance coupling model. To simplify the analysis, it is based on the following assumptions:
- The circuit is considered as high-quality factor (high Q) circuit where the inverter current (I_{in}) is sinusoid. Therefore, the first harmonic approximation (FHA) can be applied.
- Equivalent series resistance of all inductors and capacitors are neglected.
- MOSFET switches are ideal.
- The main coupling capacitance between plate P_1 and P_3 is equal to the main coupling capacitance between plate P_2 and P_4 ($C_{13}=C_{24}$).
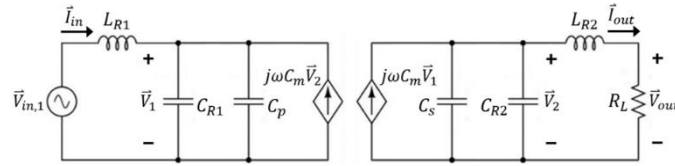- The cross-coupling capacitances (C_{14} and C_{23}) are neglected.

Figure 4. Simplified equivalent circuit of capacitive power transfer system under studied

From the first harmonic approximation, the square wave voltage (V_{in}) can be replaced by its fundamental component ($V_{in,1}$), which has the magnitude of:

$$\left|\vec{V}_{in,1}\right| = \frac{4V_{dc}}{\pi} \tag{3}$$

the primary capacitance (C_p), secondary capacitance (C_s), and mutual capacitance (C_m) can be calculated from the measured capacitance of practical capacitor of four-plates capacitive coupler as:

$$C_p = C_{12} + \frac{(C_{13}+C_{14})(C_{23}+C_{24})}{C_{13}+C_{14}+C_{23}+C_{24}} \tag{4}$$

$$C_s = C_{34} + \frac{(C_{13}+C_{23})(C_{14}+C_{24})}{C_{13}+C_{14}+C_{23}+C_{24}} \tag{5}$$

$$C_m = \frac{C_{24}C_{13}-C_{14}C_{23}}{C_{13}+C_{14}+C_{23}+C_{24}} \tag{6}$$

from (6), by neglecting the cross-coupling capacitances (C_{14} and C_{23}), the main coupling capacitances are approximately equal to:

$$C'_{13} = C'_{24} = 2C_m \tag{7}$$

the system will be operated at an angular resonant frequency (ω_o) if the resonant capacitors in both primary and secondary circuits are tuned to:

$$C_{R1} = \frac{1-C_p L_{R1}\omega_o^2}{L_{R1}\omega_o^2} \tag{8}$$

$$C_{R2} = \frac{L_{R2}-C_s L_{R2}^2 \omega_o^2 - C_s R_L^2}{L_{R2}^2 \omega_o^2 + R_L^2} \tag{9}$$

at resonance state, the output power can be obtained by:

$$P_{out} = \frac{16 R_L V_{dc}^2}{2\pi^2 L_{R1}^2 C_m^2 \omega_o^4 (R_L^2 + \omega_o^2 L_{R2}^2)} \tag{10}$$

from (10), the mutual capacitance can be derived as:

$$C'_m = \sqrt{\frac{16 R_L V_{dc}^2}{2 P_{out}\pi^2 L_{R1}^2 \omega_o^4 (R_L^2 + \omega_o^2 L_{R2}^2)}} \tag{11}$$

3. DESIGN GUIDELINE

The guideline for designing a capacitive power transfer system to achieve targeted output power is presented in this work. With use of this guideline, a suitable cross-sectional area of conductive plate used for capacitive coupler can be obtained. It has been guided through the design procedure as shown in Figure 5, which consists of 8 steps. The first step is to assign the targeted or desired output power (P_{out}). In the second step, six design constraints are defined, which are the air gap between conductive plate (d), DC input voltage (V_{dc}), resonant frequency (f_o), primary resonant inductance (L_{R1}), secondary resonant inductance (L_{R2}), and a load resistance (R_L). The third step is to calculate a mutual capacitance (C_m) which is required to achieve the

targeted output power. This can be done by using (11). In the fourth step, cross-sectional area (A) of conductive plate is calculated by using (2) and C_m obtained from the third step. The fifth step is to create a four-plates capacitive coupler according to the required cross-sectional area obtained in the previous step. In the sixth step, main coupling capacitance (C_{13} and C_{24}), cross-coupling capacitance (C_{14} and C_{23}), and leakage capacitance (C_{12} and C_{34}) of created capacitive coupler are measured. The primary capacitance (C_p), secondary capacitance (C_s), and mutual capacitance (C_m) are then calculated in the seventh step using (4) to (6) and the measured capacitances obtained in the sixth step. In the final step, primary resonant capacitance (C_{R1}) and secondary resonant capacitance (C_{R2}), which is required for the system to operate at resonance, are calculated using (8) and (9).
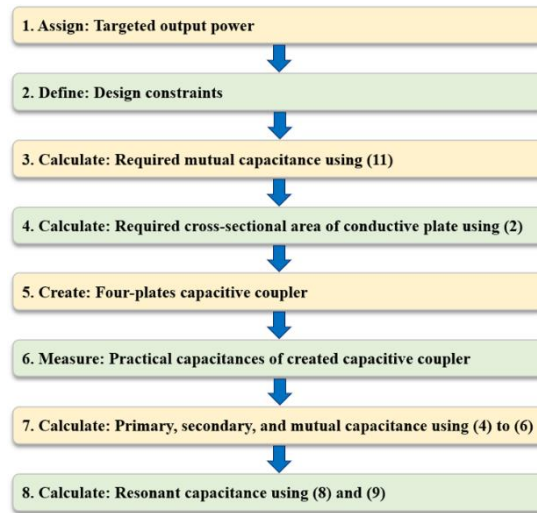

Figure 5. Design procedure of capacitive power transfer system to achieve targeted output power

4.   DESIGN EXAMPLE
To demonstrate the proposed procedure to design a capacitive power transfer system referred to Figure 5, an example of CPT system design to achieve an output power of 5-watts is presented in this section step by step.
- Step 1: in the first step, the targeted output power is assigned, which is set to 5-watts.
- Step 2: the design constraints are defined in this step, which have been listed in Table 1.

Table 1. List of design constraints

Parameters	Values
Air gap between conductive plate (d)	3 mm
DC input voltage (V_{dc})	30 V
Resonant frequency (f_o)	309 kHz
Primary resonant inductance (L_{R1})	631.02 μH
Secondary resonant inductance (L_{R2})	630.54 μH
Load resistance (R_L)	40 Ω

- Step 3: the required mutual capacitance to achieve targeted output power is calculated in this step by using (11), which is given as:

$$C'_m = \sqrt{\frac{16 R_L V_{dc}^2}{2 P_{out} \pi^2 L_{R1}^2 \omega_o^4 (R_L^2 + \omega_o^2 L_{R2}^2)}}$$

$$= \sqrt{\frac{16 \times 40 \times (30)^2}{2 \times 5 \times \pi^2 \times (631.02\mu)^2 \times (2\pi \times 309k)^4 \times [(40)^2 + (2\pi \times 309k)^2 (630.54\mu)^2]}} = 26.22 pF$$

- Step 4: in this step, the required cross-sectional area of conductive plate used for capacitive coupler corresponding to the mutual capacitance obtained in step3 is calculated by using (2), which is given as:

$$A = \frac{Cd}{\varepsilon_o \varepsilon_r} = \frac{26.22 \times 10^{-12} \times 3 \times 10^{-3}}{8.854 \times 10^{-12} \times 1} = 0.0178 \; m^2$$

to ensure that the designed capacitive coupler can transfer sufficient power, the neglected cross-coupling capacitance should be compensated by increasing the calculated cross-sectional area by 10 percent. Therefore, a 14×14 cm^2=0.0196 m^2 conductive plate has been selected.

- Step 5: four-plates capacitive coupler is created in this step using the cross-sectional area obtained in step4 (14×14 cm2), which can be shown in Figure 6.

Figure 6. Four-plates capacitive coupler created in step 5

- Step 6: six practical capacitors existing in created capacitive coupler are measured in this step using the LCR meter, which can be shown in Table 2.

Table 2. Measured capacitances of created capacitive coupler

Parameters	Values
Main coupling capacitance between P_1 and P_3 (C_{13})	59.44 pF
Main coupling capacitance between P_2 and P_4 (C_{24})	60.44 pF
Cross-coupling capacitance between P_1 and P_4 (C_{14})	7.65 pF
Cross-coupling capacitance between P_2 and P_3 (C_{23})	9.32 pF
Leakage capacitance between P_1 and P_2 (C_{12})	9.13 pF
Leakage capacitance between P_3 and P_4 (C_{34})	9.84 pF

- Step 7: the primary capacitance (Cp), secondary capacitance (Cs), and mutual capacitance (Cm) corresponding to the measured capacitances obtained in step 6 are calculated by using (4)-(6), which are given as:

$$C_p = C_{12} + \frac{(C_{13} + C_{14})(C_{23} + C_{24})}{C_{13} + C_{14} + C_{23} + C_{24}} = 9.13 \; p + \frac{(59.44p + 7.65p)(9.32p + 60.44p)}{59.44p + 7.65p + 9.32p + 60.44p} = 43.33 \; pF$$

$$C_s = C_{34} + \frac{(C_{13} + C_{23})(C_{14} + C_{24})}{C_{13} + C_{14} + C_{23} + C_{24}} = 9.84 \; p + \frac{(59.44p + 9.32p)(7.65p + 60.44p)}{59.44p + 7.65p + 9.32p + 60.44p} = 44.05 \; pF$$

$$C_m = \frac{C_{24}C_{13} - C_{14}C_{23}}{C_{13} + C_{14} + C_{23} + C_{24}} = \frac{(60.44 \; p \times 59.44 \; p) - (7.65 \; p \times 9.32 \; p)}{59.44 \; p + 7.65 \; p + 9.32 \; p + 60.44 \; p} = 25.73 \; pF$$

- Step 8: in the final step, primary resonant capacitance (CR1) and secondary resonant capacitance (CR2) are calculated by using (8) and (9), which are given as:

$$C_{R1} = \frac{1 - C_p L_{R1} \omega_o^2}{L_{R1} \omega_o^2} = \frac{1 - [43.33 \times 10^{-12} \times 631.02 \times 10^{-6} \times (2\pi \times 309k)^2]}{631.02 \times 10^{-6} \times (2\pi \times 309k)^2} = 377.09 \; pF$$

$$C_{R2} = \frac{L_{R2} - C_s L_{R2}^2 \omega_o^2 - C_s R_L^2}{L_{R2}^2 \omega_o^2 + R_L^2}$$

$$= \frac{(630.54 \times 10^{-6}) - [44.05 \times 10^{-12} \times (630.54 \times 10^{-6})^2 \times (2\pi \times 309 \, k)^2] - [44.05 \times 10^{-12} \times (40)^2]}{[(630.54 \times 10^{-6})^2 \times (2\pi \times 309 \, k)^2] + (40)^2}$$

$$= 376.24 \, pF$$

5.   EXPERIMENTAL RESULTS AND DISCUSSION

To validate the proposed design guideline, the results obtained from the design example in section 4 is implemented, which can be shown in Figure 7. A laboratory DC power supply is used as the input DC voltage source. It has been set to constant at 30 V throughout the operation. The full-bridge inverter circuit consists of four MOSFETs and a gate driver circuit. Gate signals are generated from the microcontroller unit which is the square wave pulse with 50 percent duty cycle. Their frequency is fixed at 309 kHz. The capacitive coupler is made of four copper plates with a thickness of 1.5 mm. Each plate has a dimension of 14×14 cm^2. The air gap between the plates is set to 3 mm. Note that the position of all conductive plates is fixed throughout the operation and there is no misalignment between the main coupling capacitors. The measured capacitance of capacitive coupler is already shown in Table 2. Both primary and secondary resonant inductors (L_{R1} and L_{R2}) are built based on the solenoid coil. PVC plastic with a diameter of 20.32 cm is used as a magnetic core. The 40 turns of litz-wire are wound around the core, which results in a coil length of 10 cm. Their measured inductances are shown in Table 1. Film capacitors are used as the primary and secondary resonant capacitors. Due to the availability of capacitance value in the market, both resonant capacitors are selected close to the design value which is 378 pF. The 10 W ceramic resistor is adopted as the load resistor. The experimental measurements are performed using the digital oscilloscope where the measured waveforms are shown in Figures 8 and 9. As seen in Figure 8, the waveform of inverter voltage (V_{in}) and inverter current (I_{in}) are square wave and sinusoid, respectively. Both waveforms have a frequency of 309 kHz which is the system resonant frequency. The current I_{in} is in phase with the voltage V_{in} due to the system is operated at resonance. As seen in Figure 9, the output voltage (V_{out}) and output current (I_{out}) are sinusoid and have the same phase angle. Their RMS values are measured as 13.8 V and 0.349 A, respectively. This gives the output power of 4.82 W, which is very close to the targeted value of 5 W. A small error is found to be 3.6 percent.
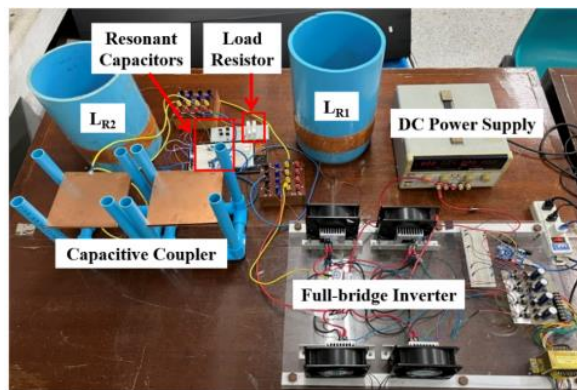

Figure 7. The experimental setup

The causes of error can be discussed as follows: i) There are the parasitic resistances in resonant inductors and capacitors which are not included in the circuit analysis; and ii) The value of resonant capacitors used in the experimental setup deviates from the design value. Therefore, to obtain better accuracy, these parasitic resistances should be as low as possible, and the resonant capacitances should be selected as close as possible to the design values.

The presented design guideline of CPT system can be summarized and discussed as follows: i) This design guideline is limited to the CPT system that has a small air gap (1–10 mm). Therefore, it is suitable for low power (5–20 W) applications, such as wireless charging for consumer electronics; ii) The four-plates capacitive coupler under studied is arranged as shown in Figure 6 with no misalignment between plates that create the main coupling capacitance. In addition, the position of all plates is fixed throughout the operation. Thus, static wireless charging applications with single position is preferred; iii) Although the distance between adjacent plates affects the value of cross-coupling and leakage capacitance, these capacitances can still be neglected if the ratio between square root of plate area and air gap ($\frac{\sqrt{A}}{d}$) is kept higher than 10. In this case, the practical parallel-plate capacitor is almost identical to the ideal capacitor where the presented design guideline is reserved.
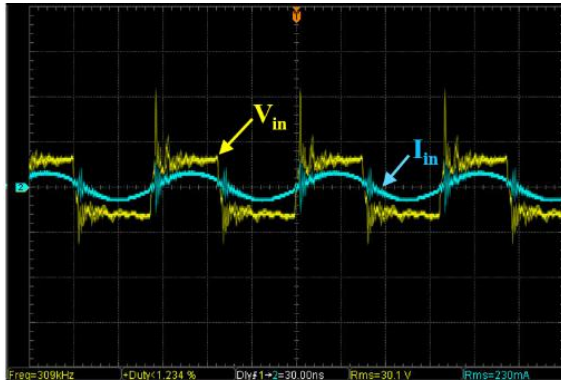
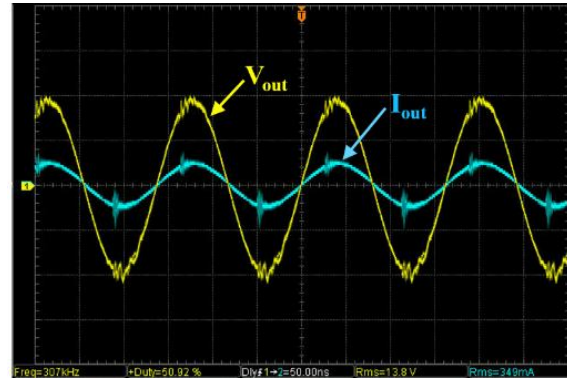Figure 8. Experimental waveforms of inverter voltage and inverter current

Figure 9. Experimental waveforms of output voltage and output current

6. CONCLUSION

A guideline to design the capacitive power transfer system to achieve a targeted output power is presented in this paper. The main objective is to obtain an accurate value of the cross-sectional area of conductive plates used for the four-plates capacitive coupler, subjected to six design constraints which are the air gap between conductive plate, DC input voltage, resonant frequency, primary resonant inductance, secondary resonant inductance, and a load resistance. The presented design procedure consists of 8 steps where each step is demonstrated through a design example of 5-watts CPT system. The experimental results indicate that the obtained output power is very close to the targeted value with a small error of 3.6 percent. This verifies the proposed design guideline.

ACKNOWLEDGEMENTS

REFERENCES

[1] N. Mohamed *et al.*, "A comprehensive analysis of wireless charging systems for electric vehicles," *IEEE Access*, vol. 10, pp. 43865–43881, 2022, doi: 10.1109/ACCESS.2022.3168727.

[2] C.-W. Chang, P. Riehl, and J. Lin, "Design and optimization of wireless charging drawer coil for smart garments," *IEEE Microwave and Wireless Components Letters*, vol. 32, no. 10, pp. 1227–1230, Oct. 2022, doi: 10.1109/LMWC.2022.3172407.

[3] Y. Jiang, K. Chen, Z. Zhao, L. Yuan, T. Tan, and Q. Lin, "Designing an M-shape magnetic coupler for the wireless charging system in railway applications," *IEEE Transactions on Power Electronics*, vol. 37, no. 1, pp. 1059–1073, Jan. 2022, doi: 10.1109/TPEL.2021.3072248.

[4] N. S. Jeong, S. Kim, H.-J. Lee, and J. H. Kim, "Wireless charging of a metal-encased device," *IEEE Transactions on Antennas and Propagation*, vol. 70, no. 1, pp. 654–663, Jan. 2022, doi: 10.1109/TAP.2021.3102023.

[5] S. Nutwong, A. Sangswang, S. Naetiladdanon, and E. Mujjalinvimut, "A novel output power control of wireless powering kitchen appliance system with free-positioning feature," *Energies*, vol. 11, no. 7, p. 1671, Jun. 2018, doi: 10.3390/en11071671.

[6] C. R. Teeneti, T. T. Truscott, D. N. Beal, and Z. Pantic, "Review of wireless charging systems for autonomous underwater vehicles," *IEEE Journal of Oceanic Engineering*, vol. 46, no. 1, pp. 68–87, Jan. 2021, doi: 10.1109/JOE.2019.2953015.

[7] J. Chen, C. W. Yu, and W. Ouyang, "Efficient wireless charging pad deployment in wireless rechargeable sensor networks," *IEEE Access*, vol. 8, pp. 39056–39077, 2020, doi: 10.1109/ACCESS.2020.2975635.

[8] Y. Yao, P. Sun, X. Liu, Y. Wang, and D. Xu, "Simultaneous wireless power and data transfer: a comprehensive review," *IEEE Transactions on Power Electronics*, vol. 37, no. 3, pp. 3650–3667, Mar. 2022, doi: 10.1109/TPEL.2021.3117854.

[9] T. Wang, Q. Xu, W. Jia, Z.-H. Mao, H. Tang, and M. Sun, "Dual-functional wireless power transfer and data communication design for micromedical implants," *IEEE Journal of Emerging and Selected Topics in Power Electronics*, vol. 9, no. 5, pp. 6259–6271, Oct. 2021, doi: 10.1109/JESTPE.2021.3049787.

[10] B. Clerckx, R. Zhang, R. Schober, D. W. K. Ng, D. I. Kim, and H. V. Poor, "Fundamentals of wireless information and power transfer: from RF energy harvester models to signal and system designs," *IEEE Journal on Selected Areas in Communications*, vol. 37, no. 1, pp. 4–33, Jan. 2019, doi: 10.1109/JSAC.2018.2872615.

[11] Z. Wang, Y. Zhang, X. He, B. Luo, and R. Mai, "Research and application of capacitive power transfer system: a review," *Electronics*, vol. 11, no. 7, p. 1158, Apr. 2022, doi: 10.3390/electronics11071158.

[12] M. Z. Erel, K. C. Bayindir, M. T. Aydemir, S. K. Chaudhary, and J. M. Guerrero, "A comprehensive review on wireless capacitive power transfer technology: fundamentals and applications," *IEEE Access*, vol. 10, pp. 3116–3143, 2022, doi: 10.1109/ACCESS.2021.3139761.

[13] Z. Zhang, H. Pang, A. Georgiadis, and C. Cecati, "Wireless power transfer—an overview," *IEEE Transactions on Industrial Electronics*, vol. 66, no. 2, pp. 1044–1058, Feb. 2019, doi: 10.1109/TIE.2018.2835378.

[14] A. N. M. S. Hossain, R. Erfani, P. Mohseni, and H. M. Lavasani, "On the non-idealities of a capacitive link for wireless power transfer to biomedical implants," *IEEE Transactions on Biomedical Circuits and Systems*, vol. 15, no. 2, pp. 314–325, Apr. 2021, doi: 10.1109/TBCAS.2021.3069842.

[15] R. Sedehi *et al.*, "A wireless power method for deeply implanted biomedical devices via capacitively coupled conductive power transfer," *IEEE Transactions on Power Electronics*, vol. 36, no. 2, pp. 1870–1882, Feb. 2021, doi: 10.1109/TPEL.2020.3009048.

[16] R. Erfani, F. Marefat, S. Nag, and P. Mohseni, "A 1–10-MHz frequency-aware CMOS active rectifier with dual-loop adaptive delay compensation and >230-mW output power for capacitively powered biomedical implants," *IEEE Journal of Solid-State Circuits*, vol. 55, no. 3, pp. 756–766, Mar. 2020, doi: 10.1109/JSSC.2019.2956883.

[17] M. Z. Bin Mustapa, S. Saat, Y. Yusof, and M. M. Shaari, "Capacitive power transfer in biomedical implantable device: a review," *International Journal of Power Electronics and Drive Systems (IJPEDS)*, vol. 10, no. 2, p. 935, Jun. 2019, doi: 10.11591/ijpeds.v10.i2.pp935-942.

[18] R. Narayanamoorthi, "Modeling of capacitive resonant wireless power and data transfer to deep biomedical implants," *IEEE Transactions on Components, Packaging and Manufacturing Technology*, vol. 9, no. 7, pp. 1253–1263, Jul. 2019, doi: 10.1109/TCPMT.2019.2922046.

[19] R. Erfani, F. Marefat, A. M. Sodagar, and P. Mohseni, "Modeling and experimental validation of a capacitive link for wireless power transfer to biomedical implants," *IEEE Transactions on Circuits and Systems II: Express Briefs*, vol. 65, no. 7, pp. 923–927, Jul. 2018, doi: 10.1109/TCSII.2017.2737140.

[20] B. Regensburger, S. Sinha, A. Kumar, S. Maji, and K. K. Afridi, "High-performance multi-MHz capacitive wireless power transfer system for EV charging utilizing interleaved-foil coupled inductors," *IEEE Journal of Emerging and Selected Topics in Power Electronics*, vol. 10, no. 1, pp. 35–51, Feb. 2022, doi: 10.1109/JESTPE.2020.3030757.

[21] V.-B. Vu, M. Dahidah, V. Pickert, and V.-T. Phan, "An improved LCL-L compensation topology for capacitive power transfer in electric vehicle charging," *IEEE Access*, vol. 8, pp. 27757–27768, 2020, doi: 10.1109/ACCESS.2020.2971961.

[22] C. Li, X. Zhao, C. Liao, and L. Wang, "A graphical analysis on compensation designs of large-gap CPT systems for EV charging applications," *CES Transactions on Electrical Machines and Systems*, vol. 2, no. 2, pp. 232–242, Jun. 2018, doi: 10.30941/CESTEMS.2018.00029.

[23] C. Cai, X. Liu, S. Wu, X. Chen, W. Chai, and S. Yang, "A misalignment tolerance and lightweight wireless charging system via reconfigurable capacitive coupling for unmanned aerial vehicle applications," *IEEE Transactions on Power Electronics*, vol. 38, no. 1, pp. 22–26, Jan. 2023, doi: 10.1109/TPEL.2022.3198529.

[24] P. K. Chittoor, B. Chokkalingam, and L. Mihet-Popa, "A review on UAV wireless charging: fundamentals, applications, charging techniques and standards," *IEEE Access*, vol. 9, pp. 69235–69266, 2021, doi: 10.1109/ACCESS.2021.3077041.

[25] C. Park *et al.*, "Separated circular capacitive coupler for ceducing cross-coupling capacitance in crone cireless cower transfer system," *IEEE Transactions on Microwave Theory and Techniques*, vol. 68, no. 9, pp. 3978–3985, Sep. 2020, doi: 10.1109/TMTT.2020.2989118.

[26] L. Yang, M. Ju, and B. Zhang, "Bidirectional undersea capacitive wireless power transfer system," *IEEE Access*, vol. 7, pp. 121046–121054, 2019, doi: 10.1109/ACCESS.2019.2937888.

[27] H. Yuan *et al.*, "A novel anti-offset interdigital electrode capacitive coupler for mobile desktop charging," *IEEE Transactions on Power Electronics*, vol. 38, no. 3, pp. 4140–4151, Mar. 2023, doi: 10.1109/TPEL.2022.3220674.

[28] N. Nabila, S. Saat, Y. Yusop, M. S. M Isa, and A. A. Basari, "The design of auto-tuning capacitive power transfer for rotary applications using phased-locked-loop," *International Journal of Power Electronics and Drive Systems (IJPEDS)*, vol. 10, no. 1, p. 307, Mar. 2019, doi: 10.11591/ijpeds.v10.i1.pp307-318.

[29] A. N. M. S. Hossain, P. Mohseni, and H. M. Lavasani, "Design and optimization of capacitive links for wireless power transfer to biomedical implants," *IEEE Transactions on Biomedical Circuits and Systems*, vol. 16, no. 6, pp. 1299–1312, Dec. 2022, doi: 10.1109/TBCAS.2022.3213000.

[30] W. Zhou, Q. Gao, R. Mai, Z. He, and A. P. Hu, "Design and analysis of a CPT system with extendable pairs of electric field couplers," *IEEE Transactions on Power Electronics*, vol. 37, no. 6, pp. 7443–7455, Jun. 2022, doi: 10.1109/TPEL.2021.3134708.

[31] L. Fang, H. Zhou, W. Hu, X. Gao, H. Liu, and Q. Deng, "Design and analysis of flexible capacitive power transfer with stable output capability," *IEEE Transactions on Circuits and Systems I: Regular Papers*, vol. 69, no. 11, pp. 4691–4701, Nov. 2022, doi: 10.1109/TCSI.2022.3194647.

[32] M. B. Lillholm, Y. Dou, X. Chen, and Z. Zhang, "Analysis and design of 10-MHz capacitive power transfer With multiple independent outputs for low-power portable devices," *IEEE Journal of Emerging and Selected Topics in Power Electronics*, vol. 10, no. 1, pp. 149–159, Feb. 2022, doi: 10.1109/JESTPE.2020.3035493.

[33] J. Lian, X. Qu, X. Chen, and C. C. Mi, "Design of a double-sided LCLC -compensated capacitive power transfer system with predesigned coupler plate voltage stresses," *IEEE Journal of Emerging and Selected Topics in Power Electronics*, vol. 10, no. 1, pp. 128–137, Feb. 2022, doi: 10.1109/JESTPE.2020.3030657.

[34] W. Zhou, Q. Gao, L. He, B. Luo, R. Mai, and Z. He, "Design of CPT system with multiple constant output voltage pickups using inverse hybrid parameters of capacitive coupler," *IEEE Transactions on Industry Applications*, vol. 58, no. 1, pp. 1061–1070, Jan. 2022, doi: 10.1109/TIA.2021.3109172.

[35] M. Kim and J. Choi, "Design of robust capacitive power transfer systems using high-frequency resonant inverters," *IEEE Journal of Emerging and Selected Topics in Industrial Electronics*, vol. 3, no. 3, pp. 465–473, Jul. 2022, doi: 10.1109/JESTIE.2021.3111528.

[36] L. Yang *et al.*, "Analysis and design of four-plate capacitive wireless power transfer system for undersea applications," *CES Transactions on Electrical Machines and Systems*, vol. 5, no. 3, pp. 202–211, Sep. 2021, doi: 10.30941/CESTEMS.2021.00024.

[37] S. Catalán Izquierdo, J. M. Bueno Barrachina, C. S. Cañas Peñuelas, and F. Cavallé Sesé, "Capacitance evaluation on parallel-plate capacitors by means of finite element analysis," *Renewable Energy and Power Quality Journal*, vol. 1, no. 07, pp. 613–616, Apr. 2009, doi: 10.24084/repqj07.451.

[38] L. Huang and A. P. Hu, "Defining the mutual coupling of capacitive power transfer for wireless power transfer," *Electronics Letters*, vol. 51, no. 22, pp. 1806–1807, Oct. 2015, doi: 10.1049/el.2015.2709.

[39] B. Minnaert and N. Stevens, "Design of a capacitive wireless power transfer link with minimal receiver circuitry," in *2018 IEEE PELS Workshop on Emerging Technologies: Wireless Power Transfer (Wow)*, Jun. 2018, pp. 1–5, doi: 10.1109/WoW.2018.8450659.

[40] J. Lian and X. Qu, "Design of a double-sided LC compensated capacitive power transfer system with capacitor voltage stress optimization," *IEEE Transactions on Circuits and Systems II: Express Briefs*, vol. 67, no. 4, pp. 715–719, Apr. 2020, doi: 10.1109/TCSII.2019.2918648.

BIOGRAPHIES OF AUTHORS

Supapong Nutwong 🆔 🔍 ᴄ 🗨 is a lecturer in Electrical Engineering Department, Faculty of Engineering, King Mongkut's University of Technology Thonburi (KMUTT), Bangkok, Thailand since 2020; He received the B.Eng. degree and M.Eng. degree in Electrical Engineering from the King Mongkut's University of Technology Thonburi in 2007 and 2011, respectively; and the D.Eng. degree in Electrical and Information Engineering Technology from the King Mongkut's University of Technology Thonburi in 2019. From 2013 to 2014, he was a Researcher at the Educational Support Unit, KMUTT. Since 2022, he has been an Assistant Professor with the Department of Electrical Engineering, KMUTT. His research interests include the field of power electronics, inductive power transfer (IPT) systems, capacitive power transfer (CPT) systems, wireless charging applications, and induction heating systems. He can be contacted at email: supapong.nut@kmutt.ac.th.

Ekkachai Mujjalinvimut 🆔 🔍 ᴄ 🗨 is a lecturer in Electrical Engineering Department, Faculty of Engineering, King Mongkut's University of Technology Thonburi (KMUTT), Bangkok, Thailand since 2016; He received the B.Eng. degree and M.Eng. degree in Electrical Engineering from the King Mongkut's University of Technology Thonburi in 2007 and 2009, respectively; and the D.Eng. degree in Electrical and Information Engineering Technology from the King Mongkut's University of Technology Thonburi in 2016. Since 2019, he has been an Assistant Professor with the Department of Electrical Engineering, KMUTT. His current research interests include switched mode power supplies, applications of nonlinear control theory, and digital control. He can be contacted at email: ekkachai.muj@kmutt.ac.th.

Anawach Sangswang 🆔 🔍 ᴄ 🗨 is a lecturer in Electrical Engineering Department, Faculty of Engineering, King Mongkut's University of Technology Thonburi (KMUTT), Bangkok, Thailand; He received the B.Eng. degree in Electrical Engineering from the King Mongkut's University of Technology Thonburi in 1995; and the M.Sc. and Ph.D. degrees in Electrical Engineering from Drexel University, Philadelphia, PA, in 1999 and 2003, respectively. Since 2020, he has been an Associate Professor with the Department of Electrical Engineering, KMUTT. From 1999 to 2003, he was a Research Assistant with the Center for Electric Power Engineering, Drexel University. His research interests include induction heating, wireless power transfer, energy management systems, and power system stability. He can be contacted at email: anawach.san@kmutt.ac.th.

Nattapong Hatchavanich 🆔 🔍 ᴄ 🗨 is a lecturer in Electrical Engineering Department, Faculty of Engineering, King Mongkut's University of Technology Thonburi (KMUTT), Bangkok, Thailand since 2021; He received the B.Eng. degree in Electrical Engineering from the King Mongkut's University of Technology North Bangkok (KMUTNB) in 2012; received the M.Eng. degree in Electrical Engineering from the King Mongkut's University of Technology Thonburi in 2016; and the D.Eng. degree in Electrical and Information Engineering Technology from the King Mongkut's University of Technology Thonburi in 2020. His current research interests include the resonant inverter and control technique for wireless power transfer system (WPT) and induction heating applications. He can be contacted at email: nattapong.hat@kmutt.ac.th.

Mongkol Konghirun 🆔 🔍 ᴄ 🗨 is a lecturer in Electrical Engineering Department, Faculty of Engineering, King Mongkut's University of Technology Thonburi (KMUTT), Bangkok, Thailand; He received the B.Eng. degree (First Class Honors) in Electrical Engineering from the King Mongkut's University of Technology Thonburi in 1995; and the M.Sc. and Ph.D. degrees in Electrical Engineering from The Ohio State University, Columbus, OH, USA, in 1999 and 2003, respectively. Presently, he is an Associate Professor with the Department of Electrical Engineering, King Mongkut's University of Technology Thonburi. His research interests include electric motor drives, power electronics, railway electrification, and renewable energy. He can be contacted at email: mongkol.kon@kmutt.ac.th.